The Layered Lanthanum Carbide Halide Superconductors $La_2C_2(X,X')_2$ (X,X′ = Cl, Br, I): Neutron Powder Diffraction Characterization and Electronic Properties

Kyungsoo Ahn, Brendan J. Gibson, Reinhard K. Kremer, Hansjürgen Mattausch, Andres Stolovits,† and Arndt Simon*

Max-Planck-Institut für Festkörperforschung, Heisenbergstrasse 1, D-70569 Stuttgart

Received: December 7, 1998; In Final Form: April 20, 1999

The superconducting properties of $La_2C_2(X, X')_2$(X, X′ = Cl, Br, I) are investigated. Three different samples of $La_2C_2Br_2$, which are obtained under different synthesis conditions, show superconductivity at 7.03(5) K. $La_2C_2I_2$ ($T_c \approx 1.7$ K) exhibits slightly different transition temperatures for differently prepared samples. A total of five samples of $La_2C_2(X, X')_2$ were investigated by high resolution neutron powder diffraction from room temperature to 1.5 K. Rietveld refinements yield the structural parameters, in particular of the C atoms. These allow us to follow in detail the variation of the interatomic distance in the C_2 group. On the basis of the low temperature structural parameters, extended Hückel band structure calculations were performed and a band of low dispersion along the Γ−N direction in the Brillouin zone was identified. We discuss correlations of structural and electronic properties with the superconducting transition temperatures of the $La_2C_2(X, X')_2$ phases.

I. Introduction

In the course of our search for new superconductors, we found superconductivity up to 11.6 K in the layered rare-earth metal carbide halides $RE_2C_2X_2$ (RE = Y, La; X = Cl, Br, I).[1] They crystallize in the $Gd_2C_2Br_2$ structure types.[2,3] Therein C−C units are located in the octahedral voids in close packed metal atom double layers. The latter are sandwiched between layers of halogen atoms. Such slabs are connected via the van der Waals interaction. Different stacking sequences (1s and 3s stacking variants) are found (Figure 1). Superconductivity in layered halide phases was reported for alkali metal intercalated Hf and Zr nitride chlorides reaching transition temperatures up to 25.5 K.[4−6]

Considerable work has been devoted to an investigation of the superconducting properties of the yttrium-based phases of the rare-earth metal carbide halides.[7−13] The experiments done on the $Y_2C_2X_2$ system have revealed a number of essential experimental facts. For example, it has been demonstrated that by a proper adjustment of the ratio of Br:I ≈ 1:3, the superconducting transition temperature in samples of $Y_2C_2(Br, I)_2$ can be maximized to 11.6 K.[7,12] An increase of the transition temperature of $Y_2C_2Br_2$ ($T_c = 5.05$ K) by about 1.2 K can also be achieved by an intercalation of Na atoms into the van der Waals gap between the double layers of halogen atoms.[11,12] A comparison with the superconducting properties of the dicarbide YC_2 (CaC_2 structure type) has shown that the pronounced structural anisotropy in the yttrium carbide halides leads to a significant increase of the electron−phonon coupling strength.[9,10] The upper critical fields in the layered yttrium carbide halides are enlarged by almost two orders of magnitude as compared to YC_2. The carbon isotope effect in YC_2 and $Y_2C_2Br_2$ is, as well, surprisingly different: While a $^{12}C/^{13}C$ isotope effect in good agreement with BCS theory has been detected in YC_2, there is no indication of a decrease of T_c when ^{13}C is substituted into $Y_2C_2Br_2$.[9,14,15]

The chemical bonding of the C−C dumbbell located in a (distorted) octahedral cage of metal atoms in the crystal structure of $RE_2C_2X_2$ phases was suggested to play an important role for superconductivity. Metallic character of the rare-earth carbide halides results from covalent overlap of the C_2-π^* and the metal atom d-orbitals.[16] Neutron powder diffraction measurements on $Y_2C_2X_2$ (X = Br, I)[9,17] revealed a slightly reduced C−C double bond distance. Raman spectroscopy on crystallites of a series of samples of $RE_2C_2X_2$ (RE = Y, Gd; X = Br, I) proves that the specific stretching and tilting vibrations of the C−C group are well decoupled from the vibrations of the heavy metal atoms forming the surrounding cage.[17] Band structure calculations for $Gd_2C_2Cl_2$[16] and $Y_2C_2Br_2$[7] point to a band of low dispersion along a certain direction in the Brillouin zone. This "flat" band being located close to the Fermi energy reflects the anisotropy of the crystal structure. Nonlinearities in the temperature dependence of the ^{13}C-NMR Korringa relaxation rate in $Y_2C_2Br_2$ and $Y_2C_2I_2$ were explained within the scope of this band structure scheme.[13]

In a first study on the $La_2C_2X_2$ (X= Cl, Br, I) system, we experienced a somewhat different behavior to that found for the $Y_2C_2X_2$ compounds.[18] In contrast to the behavior of the yttrium system, samples of $La_2C_2Br_{2-x}I_x$ show lower T_cs when the iodine content x is raised. $La_2C_2I_2$ does not show superconductivity above 2 K, while mixed I-Cl phases are superconductors with T_cs up to 3.7 K. $La_2C_2Cl_2$ itself could not be synthesized yet.

Here, we present a detailed investigation of the low temperature structural and superconducting properties of $La_2C_2Br_2$, $La_2C_2I_2$ (1s and 3s type), $La_2C_2Br_{0.5}I_{1.5}$, and $La_2C_2Cl_{0.5}I_{1.5}$. The low temperature crystal structural properties were studied employing high resolution neutron powder diffraction. Neutron diffraction was particularly useful to gain precise positional parameters of the carbon atoms. Subsequently, the refined structural parameters were used as input for an extended Hückel tight-binding calculation of the band structures.

* Prof. Dr. A. Simon: e-mail, ahn@simaix.mpi-stuttgart.mpg.de.
† Permanent address: Institute of Physics, Tartu University, Riia 142 EE-2400 Tartu, Estonia.

10.1021/jp984646d CCC: $18.00
Published on Web 06/15/1999

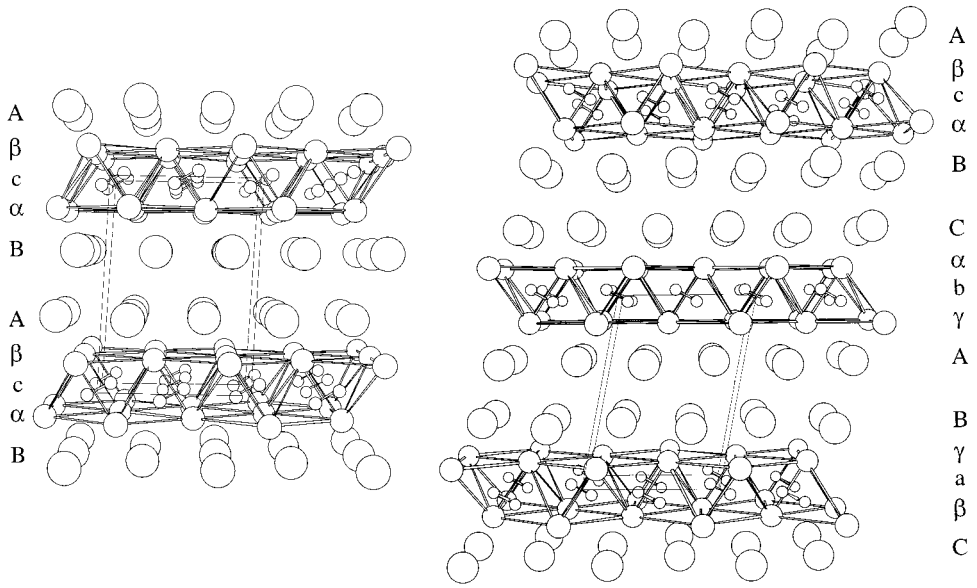

Figure 1. Perspective view of the crystal structures of $La_2C_2I_2$ (1s stacking variant left and 3s stacking variant right). I, La, and C atoms are drawn with decreasing diameter, respectively. Stacking sequences are indicated and unit cells outlined.

II. Experimental Details

A. Sample Preparation. Samples of $La_2C_2X_2$ (X= Br, I) were prepared from La metal (Johnson Matthey Inc., 99.99 %), LaX_3, and glassy carbon powder in ≈10 g batches. The trihalides LaX_3 (X = Cl, Br) were prepared from La_2O_3 (Johnson Matthey Inc., 99.9%) and NH_4X according to procedures described elsewhere,[19,20] while LaI_3 was prepared from La metal and I_2.[21] All trihalides were purified by repeated distillations in high vacuum. The carbon powder (Aldrich, 99.99%) was heated and degassed (1050 °C, 10^{-5} mbar) for 3 days and subsequently stored in a dried argon atmosphere. In order to prepare 1s-$La_2C_2X_2$, stoichiometric mixtures with a 2% excess of carbon powder were sealed in welded Ta tubes and heated to 980 °C and 1050 °C in the case of X = Br and X = I, respectively. The product for X = I contained up to ≈10% of 3s-$La_2C_2I_2$. An increased carbon excess (≈10%) was found necessary to obtain the 3s-$La_2C_2I_2$ type. Halogen mixed phases were obtained from appropriate mixtures of the metal, the trihalides, and 2% carbon excess. The reaction period was about two weeks for all samples. Two samples (1 and 2) of $La_2C_2Br_2$ were prepared from $LaBr_3$ and La_2C_3. Details of the preparation of La_2C_3 are given elsewhere.[18] We used 3% less carbon for sample 1 and 3% excess carbon for sample 2. Sample 3 was obtained from a reaction of La metal, $LaBr_3$, and 15% excess carbon powder. Since the trihalides and the reaction products are sensitive to moisture, all handling was done under dried argon gas atmosphere. The reactions yield polycrystalline material with brownish luster for $La_2C_2Br_2$ and with bronze color for the iodide and the mixed phases. The 3s-$La_2C_2I_2$ samples were found to form into thin platelets up to 2 mm in diameter.

B. Resistivity Measurements. Electrical resistivity was determined on sintered pellets of 5 mm diameter and a thickness of about 1 mm by the van der Pauw method in fields up to 7 T using the cryostat of an MPMS magnetometer (Quantum Design). Currents of 10 mA (dc) or less were supplied by a Keithley 2400 sourcemeter. The voltage drop across the contacts was determined by a HP 34420A nanovoltmeter. The pellets were enclosed into a vacuum tight copper can and pressed onto four gold plated spring pins.

C. Magnetic Susceptibility Measurements. The magnetic susceptibilities of powder samples (≈100 mg) were measured with an MPMS SQUID magnetometer between 2 and 10 K in an external field of 1 mT. The samples were contained in dried quartz glass ampoules under 1 bar He exchange gas to provide sufficient thermal contact. The sample containers were designed to give a negligible magnetic background signal.

Below 2 K ac magnetic susceptibilities were determined in a home-built top-loading single-shot ^{3}He bath glass cryostat. The ac coils being immersed in the pumped ^{4}He outer bath and held at constant temperature were operated at a frequency of 37 Hz and generated ac fields of about 0.3 mT. The design of the cryostat allows rapid mounting of the samples and is therefore particularly suited for measurements on very air and moisture sensitive rare-earth metal carbide halides. Samples of about 200 mg were pressed into cylindrical pellets to reduce the active surface of the samples. To protect the pellets during mounting they were enclosed in gelatin capsules (5 mm diameter, 12 mm length) which had been desiccated in high vacuum for 24 h.

The temperature of the ^{3}He bath was determined with a calibrated Ge resistor (Lake Shore) being in close contact with the sample. The coil setup was calibrated against a standard Al sample.

D. X-Ray Powder Diffraction. The product phases were characterized using powder X-ray diffraction measurements either with the modified Guinier technique[22] or a STOE powder diffractometer. Calibration of the lattice parameters (see Table 1) was done with Si as an external standard.

E. Neutron Powder Diffraction. Neutron powder diffraction measurements were performed with the D1A powder diffractometer (λ = 191.1 pm) at the ILL (Grenoble, France). High resolution patterns ($6° < 2\Theta < 160°$, steps of 0.05°) were collected on microcrystalline powder samples of about 10 g which were either encapsulated in thin-walled vanadium containers (i.d. 8 mm) or in quartz glass tubes (o.d. 8 mm, wall thickness < 0.5 mm). Dried helium at 1 bar was used in the ampoules as heat exchange gas.

Structure refinements from the powder patterns were carried out with the FAT-Rietan 97 program.[23] From the 2659 data points containing 216 contributing reflections, 27 parameters were refined, of which 13 were global (1 instrumental, 6 background parameters, 5 profile parameters, 1 asymmetry parameter) and 14 local (1 overall scale factor, 4 lattice

TABLE 1: Lattice Parameters at Room Temperature According to X-Ray Powder Diffraction Measurements of All Investigated Samples

no.	compd	type	*a* (pm)	*b* (pm)	*c* (pm)	β (deg)
1	$La_2C_2Br_2$	1s	745.1(3)	405.6(1)	1002.6(2)	94.31(3)
2	$La_2C_2Br_2$	1s	749.6(3)	405.9(1)	1007.0(2)	94.12(4)
3	$La_2C_2Br_2$	1s	747.4(1)	406.08(8)	1005.1(1)	94.27(2)
4	$La_2C_2I_2$	1s	764.4(3)	413.8(1)	1077.6(3)	93.10(4)
5	$La_2C_2I_2$	3s	762.4(2)	414.1(1)	1090.3(3)	100.74(4)
6	$La_2C_2Br_{0.5}I_{1.5}$	1s	760.4(1)	410.9(1)	1071.4(1)	93.40(1)
7	$La_2C_2Cl_{0.5}I_{1.5}$	1s	758.9(1)	408.61(5)	1075.2(2)	93.42(1)
8	La_2C_2BrI	1s	760.5(5)	408.4(1)	1061.8(3)	93.14(3)

TABLE 2: Parameters Used for the Extended Hückel Band Structure Calculations

element	orbital	H_{ii}	ζ_1^a	ζ_2^a	c_1^b	c_2^b
La	6s	−7.67	2.140			
	6p	−5.01	2.080			
	5d	−8.21	3.780	1.381	0.7765	0.4586
I	5s	−18.0	2.679			
	5p	−12.7	2.322			
C	2s	−21.4	1.625			
	2p	−11.4	1.625			

[a] Coefficients used in double ζ expansion. [b] Slater-type orbital exponents.

TABLE 3: Superconducting Transition Temperatures of the Investigated $La_2C_2X_2$ Samples Determined from dc and ac Susceptibility Measurements (T_c^{on}: onset temperature; T_c^{mid}: midpoint temperature)

no.	compd	type	method	T_c^{on} (K)	T_c^{mid} (K)
1	$La_2C_2Br_2$	1s	dc	6.97(5)	6.0(1)
2	$La_2C_2Br_2$	1s	dc	7.01(5)	6.3(1)
3	$La_2C_2Br_2$	1s	dc	7.03(5)	6.83(5)
4	$La_2C_2I_2$	1s	ac	1.60(5)	1.55
5	$La_2C_2I_2$	3s	ac	1.72(5)	1.65
6	$La_2C_2Br_{0.5}I_{1.5}$	1s	ac	1.65(3)	1.09
7	$La_2C_2Cl_{0.5}I_{1.5}$	1s	ac	1.82(3)	1.70
8	La_2C_2BrI	1s	ac	1.45(8) (2.3(1))	1.0

constants, 6 positional, and 3 isotropic displacement parameters). Profile matching was achieved using a pseudo-Voigt function.

III. Band Structure Calculation

The extended Hückel method[24,25] was used for the band structure calculations on $La_2C_2I_2$ using the crystal structure parameters as refined from the powder neutron diffraction measurements (Table 2). The calculations were performed on a 588 *k*-point mesh for the monoclinic cell. The electronic density of states obtained from the band structure was smoothed with Gaussians of a half-width of 0.02 eV. Band dispersion was calculated for selected directions in the Brillouin zone for 40 discrete *k*-points in each direction.

IV. Results and Discussion

A. Superconducting Properties. As verified on three different samples, 1s-$La_2C_2Br_2$ becomes superconducting below 7.03(5) K (onset temperature T_c^{on} from dc susceptibility, see Table 3). Figure 2 displays the electrical resistivity and the dc susceptibilities of a 1s-$La_2C_2Br_2$ (sample 2) which is monophasic according to a neutron powder diffraction study.[26] Zero resistivity is reached at 7.03(5) K. Diamagnetic shielding is complete while the Meissner fraction is only about 10% of the expected value. This difference is frequently observed and may be attributed to strong pinning effects at grain boundaries or crystal imperfections in the individual sample. The electrical resistivity shows a remarkable convex temperature dependence at high

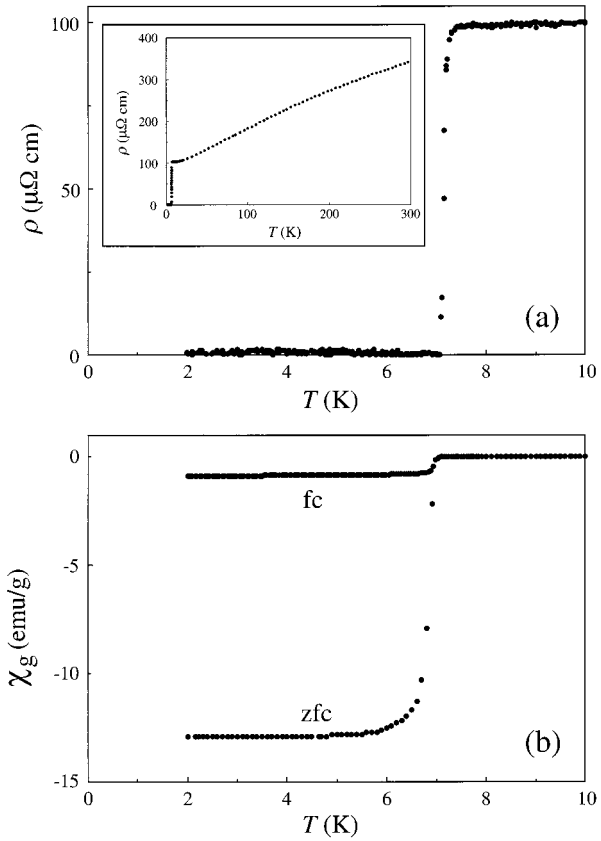

Figure 2. Electrical resistivity (a) and dc magnetic susceptibility (b) of $La_2C_2Br_2$ (sample 2). The inset in (a) displays the high temperature resistivity. In (b) fc and zfc refer to field cooled and zero-field cooled susceptibility, respectively.

temperatures (see the inset Figure 2a) which may hint at an additional scattering mechanism, e.g., a narrow band near E_F[27] which is also evidenced from the band structure calculations (see below).

Figure 3 displays the electrical resistivity in magnetic fields of a sample of $La_2C_2Br_2$ (sample 3). Magnetic fields shift the superconducting transition to lower temperatures. The absolute resistivity is by a factor of 400 larger than in sample 2, and zero resistivity is reached at a somewhat lower temperature (6.60(5) K). This noticeable difference between the two samples is attributed to the considerable amount of excess carbon in sample 3.

Using a 10% criterion as a measure for the upper critical field, we estimate $B_{c2}(0\ K)$ by an extrapolation with an even polynomial of fourth degree to be 5.6(2) T and 4.3(2) T for samples 3 and 2, respectively (see Figure 4). According to these results the upper critical field of $La_2C_2Br_2$ is somewhat higher than of isoelectronic $Y_2C_2Br_2$ (3.0(2) T, $T_c = 5.05$ K).[9]

We note the positive curvature of the phase boundary line of both samples close to $T_c(0)$. This behavior is similar to results

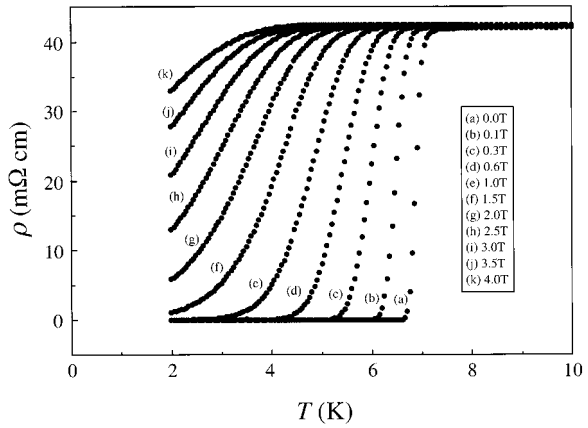

Figure 3. Resistivity of sample 3 measured in external magnetic fields as indicated.

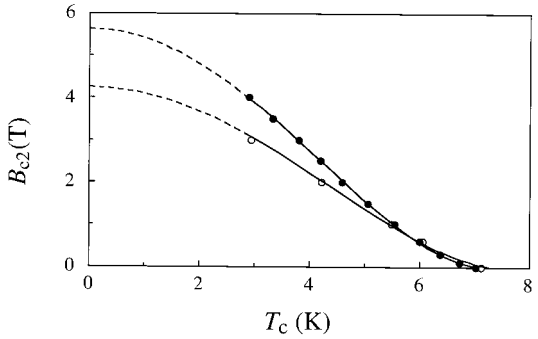

Figure 4. Upper critical field of samples 2 (○) and 3 (●) determined from a 10% drop criterion from the normal resistivity. Full lines are fits to an even polynomial in T_c (see text).

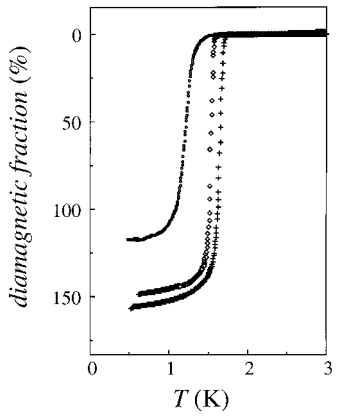

Figure 5. ac susceptibility of a sample of 1s-$La_2C_2I_2$ (○, not sintered pellet; ◇, sintered pellet) and 3s-$La_2C_2I_2$ (+) (sample 4 and 5, respectively).

found for other highly anisotropic systems such as intercalation compounds of TaS_2[28] or the organic superconductor (BEDT-TTF)$_2$Cu(NCS)$_2$ with BEDT-TTF being *bis*(ethylenedithio)-tetrathiafulvalene.[29] It has also been seen in high T_c cuprate superconductors.[30]

Figure 5 displays the ac susceptibilities of samples of 1s-$La_2C_2I_2$ and 3s-$La_2C_2I_2$ (samples 4 and 5 in Table 3). The transition to superconductivity occurs at temperatures below 2 K. This is why these transitions had been missed in our previous investigations.[18] For both samples the transitions to superconductivity are remarkably sharp. The transition width was considerably reduced by additionally sintering the pressed pellets. In contrast to $La_2C_2Br_2$, the two differently prepared samples, exhibiting 1s and 3s stacking, respectively, show a

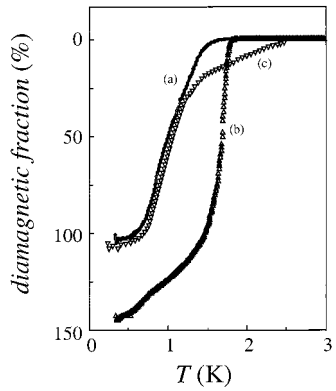

Figure 6. ac susceptibility of a sample of (a) $La_2C_2Br_{0.5}I_{1.5}$, (b) $La_2C_2Cl_{0.5}I_{1.5}$, and (c) La_2C_2BrI (sample 6, 7, and 8, respectively).

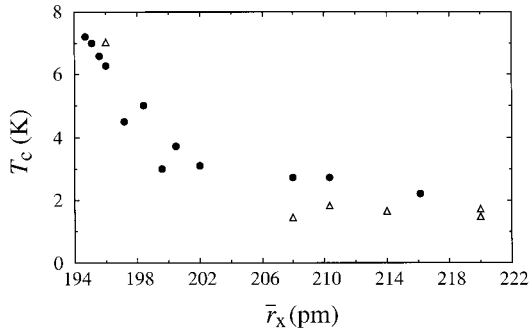

Figure 7. Transition temperatures versus the mean ionic radius $\bar{r}$ of the halogen constituents in the systems $La_2C_2(X, X')_2$(X = Cl, Br, I). △ give the results of this work; data represented by ● were taken from ref 18.

slight difference in the onset temperature $\Delta T_c^{on} \approx 0.12(5)$ K. Flux exclusion is complete at lowest temperatures for both samples as can be concluded from the comparison with an Al standard sample.

Figure 6 displays the ac susceptibilities of three samples with mixed halogen constituents (samples 6, 7, and 8 in Table 3), which are all of the 1s stacking type. The onset transition temperatures for samples 7 and 8 are higher than for 1s-$La_2C_2I_2$. This finding confirms the trend established before that replacement of I by Br or Cl raises T_c.[18]

The superconducting transition temperature of a sample of La_2C_2BrI (sample 8) which had been investigated before and had been found at 2.7 K, according to the present study is somewhat lower and appears at 2.32(5) K.[18] However, a second, even sharper transition with onset at about 1.5 K and midpoint at ≈1 K is seen which could indicate that this sample is inhomogeneous even though impurity phases were not visible in the X-ray powder diffraction pattern. There is also indication of an inhomogeneity of sample 7 not obvious from the structure investigation. However, the bulk exhibits a sharp transition.

Figure 7 displays the transition temperatures of the systems $La_2C_2(X,X')_2$ as a function of the averaged halide ion radius. Our results extend the data range of our previous publication and confirm the monotonic decrease with increasing halide ion radius. The good correlation of the experimental data into a narrow band supports our finding for the $Y_2C_2(X,X')_2$ system that, to first approximation, the averaged halide ion radius may be taken as a suitable parameter to describe the superconducting transition temperature in the $RE_2C_2X_2$ compounds. In contrast to the $Y_2C_2(X,X')_2$ system, however, we observe no local maximum in the superconducting transition temperatures of the $La_2C_2(X,X')_2$ compounds.[7,12] If we assume such a maximum

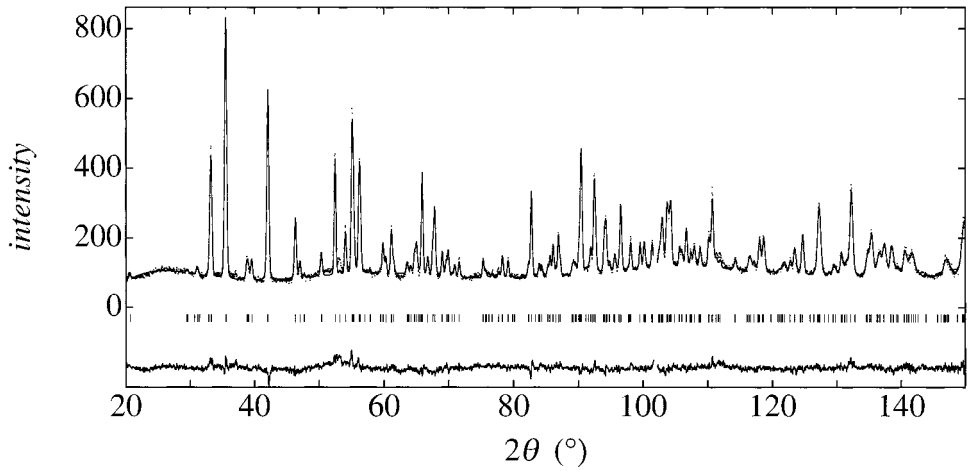

Figure 8. Observed (●), calculated (full line), and difference pattern for $La_2C_2I_2$ (3s type) at 1.5 K. Vertical bars indicate the positions of the reflections used to simulate the pattern. The broad feature in the background at low angles is due to diffuse scattering from the quartz glass container.

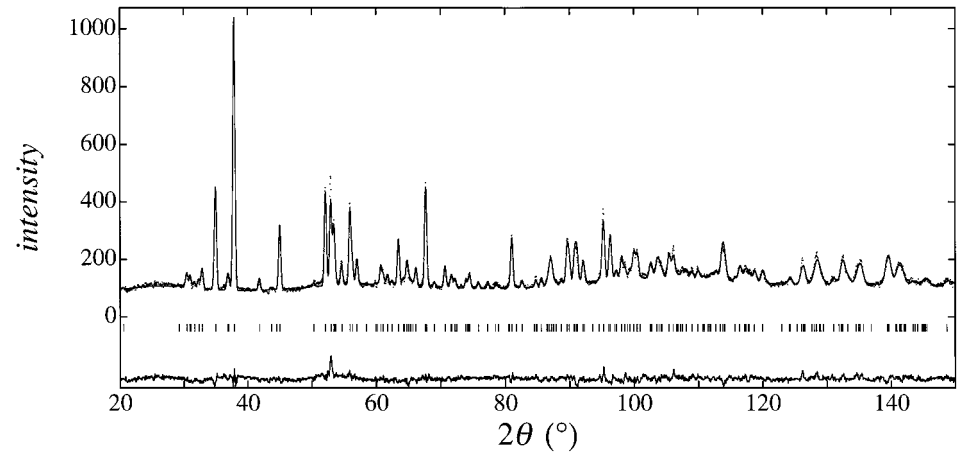

Figure 9. Observed (●), calculated (full line), and difference pattern for $La_2C_2Cl_{0.5}I_{1.5}$ (1s type) at 1.5 K. Vertical bars indicate the positions of the reflections used to simulate the pattern. The broad feature in the background at low angles is due to diffuse scattering from the quartz glass container.

TABLE 4: Positional Parameters for $La_2C_2X_2$ (X = Br, I) as Refined from the Neutron Powder Diffraction Patterns Collected at 1.5 K[a]

no.	compd	atom	*x*	*z*	B_{eq} (10^4 pm^2)
		La	0.1447(4)	0.1567(4)	0.5(1)
2	1s-$La_2C_2Br_2$	Br	0.1717(5)	0.6554(5)	0.5(1)
		C	0.4280(4)	0.0364(5)	1.5(1)
		La	0.1425(3)	0.1396(4)	0.2(1)
4	1s-$La_2C_2I_2$	I	0.1752(5)	0.6573(4)	0.2(1)
		C	0.4258(4)	0.0292(3)	0.2(1)
		La	0.4069(2)	0.1408(4)	0.1(1)
5	3s-$La_2C_2I_2$	I	0.7952(4)	0.3428(3)	0.2(1)
		C	0.0819(3)	0.0284(2)	0.4(1)

[a] The R_{wp} factors (R_p factors) amounted to 5.9% (4.6%), 10.8% (8.5%), and 5.6% (4.3%) for ls-$La_2C_2Br_2$ (no. 2), 1s-$La_2C_2I_2$ (no. 4), and 3s-$La_2C_2I_2$ (no. 5), respectively.

to exist, the transition temperatures of the $La_2C_2(X,X')_2$ compounds already lie on the descending branch above the local maximum.

B. Neutron Diffraction. The neutron powder diffraction patterns were refined on the basis of the space group *C*2/*m* (no. 12) with all atoms in position *4i* in Wyckoff notation (cf. Tables 4 and 5) of the structure for $Gd_2C_2Br_2$, either in its 1s or 3s stacking variant.[2,3] Initially, the Rietveld refinements had been started assuming the simultaneous presence of the 1s- and the 3s- $Gd_2C_2Br_2$ structure type. These first calculations proved all compounds to adopt the 1s type, except $La_2C_2I_2$, which crystallizes with both structure variants. Refinements of the patterns of two different samples of $La_2C_2I_2$ revealed exclusively the 3s type for one sample but a phase mixture of 0.92:0.08 for the 1s:3s type for the second sample. Single phase refinements of all patterns were carried out where appropriate (see Figures 8 and 9).

All samples showed no evidence for impurity phases, e.g., starting materials or decomposition products above the level of sensitivity of powder diffraction measurements. For mixed halide samples the occupation factors were also refined, and the resulting composition was found to be in good agreement with the values expected from the initial ratio of the trihalides in the starting mixtures (see Table 5). Most likely, because of the significant ion size mismatch and the concomitant local lattice stress, the isotropic thermal displacement parameters for the halogen atoms in the sample of $La_2C_2Cl_{0.51(3)}I_{1.49(3)}$ were found to be unusually large. On cooling from room temperature to 1.5 K, apart from a monotonic decrease of the lattice parameters (cf. Table 6 and 7), no indications for structural phase transitions were observed in the diffraction patterns of all samples. The C−C distance within error bars is independent of temperature. The experience with the preparation of 1s- and 3s-$La_2C_2I_2$ suggests the possibility that the C_2 group might, to

TABLE 5: Positional Parameters and Occupation Factors for $La_2C_2X_{0.5}I_{1.5}$ (X = Cl, Br) as Refined from the Neutron Powder Diffraction Patterns Collected at 1.5 K[a]

no.	compd	atom	occup	*x*	*z*	B_{eq} (10^4 pm^2)
6	1s-$La_2C_2Br_{0.5}I_{1.5}$	La	1	0.1434(2)	0.1419(1)	0.4(1)
		I	0.74(3)	0.1750(3)	0.6615(3)	0.8(1)
		Br	0.26(3)	0.1750(3)	0.6615(3)	0.8(1)
		C	1	0.4264(3)	0.0297(2)	0.6(1)
7	1s-$La_2C_2Cl_{0.5}I_{1.5}$	La	1	0.1449(3)	0.1409(2)	0.5(1)
		Cl	0.74(2)	0.1730(3)	0.6674(3)	1.9(1)
		I	0.26(2)	0.1730(4)	0.6674(3)	1.9(1)
		C	1	0.4280(3)	0.0298(2)	0.8(1)

[a] The R_{wp} factors (R_p factors) amounted to 8.8% (6.8%) and 4.8% (3.8%) for 1s-$La_2C_2Br_{0.5}I_{1.5}$ and for 1s-$La_2C_2Cl_{0.5}I_{1.5}$, respectively.

TABLE 6: Temperature Dependence of the Lattice Parameters of $La_2C_2Cl_{0.5}I_{1.5}$ (no. 7) According to Neutron Powder Diffraction

T (K)	*a* (pm)	*b* (pm)	*c* (pm)	β (deg)	d_{C-C} (pm)
1.5	758.57(3)	409.81(2)	1067.82(5)	93.272(2)	131.5(4)
10	758.55(3)	409.81(2)	1067.76(5)	93.273(2)	131.9(4)
293	761.09(4)	411.01(2)	1072.34(6)	93.268(3)	131.6(5)

some extend, be replaced by single C atoms which would occupy the centers of the metal atom octahedra. Rietveld refinements assuming this structure model, however, failed to reveal scattering density in the center of the octahedra beyond the level of sensitivity of the method. According to the calculations, the replacement of C_2 by C amounts to 0.3(6)%.

It has been pointed out in previous investigations[7,17] that the C−C bond length in the $RE_2C_2X_2$ phases is considerably reduced as compared to that commonly found for a C−C double bond observed, e.g., in ethene (d_{C-C} = 133 pm).[31] However, the C−C bond length in the La carbide halides spans a somewhat wider range than found in the Y carbide halides $Y_2C_2X_2$ (X = Br,I) phases (see Table 7).

A central question we pursued with our investigations was to reveal correlations between the structural and the superconducting (viz. electronic) properties. According to our results there is, however, no direct correlation of the transition temperatures with the C−C distances. As a general trend we rather observe an increase of the superconducting transition temperatures with decreasing distance of the axial (end-on to C_2) La atoms to closest halogen atoms in the crystal structure and also with the distance of the axial La atoms to the carbon atoms (Figure 10). All 1s type samples come to lie very close to a straight line in a $d_{La-\bar{X}}$ versus d_{La-C} plot, while the change of the stacking variant from 1s to 3s in the case of $La_2C_2I_2$ gives rise to a much increased d_{La-C} distance. A close correlation of the superconducting transition temperatures with the mean ionic radius of the halogen constituents has already been reported for the phases $Y_2C_2(X,X')_2$ and $La_2C_2(X, X')_2$ (X, X′ = Cl, Br, I),[7,18] whereas a correlation of the transition temperatures with the La−C interatomic distances has not been described before. Figure 10, in addition, indicates to first order a linear dependence of the interatomic distances of the axial La to the halogen atoms and of the distances of the La to the C atoms.

C. Band Structure Calculations. Within the Zintl−Klemm concept, the chemical bonding for the phases $RE_2C_2X_2$ may be approximated by the formula $(RE^{3+})_2C_2^{4-}(X^-)_2$, suggesting semiconducting behavior. From the molecular point of view, the metallic behavior has been attributed to backbonding from occupied $C_2-\pi^*$ to empty d-states of the metal atoms.[7,16]

The metallic character of $La_2C_2X_2$ (X = Br, I) is verified by the results of our extended Hückel calculations. Figure 11 displays the total density of states (DOS) calculated for the observed crystal structure of the 3s type of $La_2C_2I_2$. From the

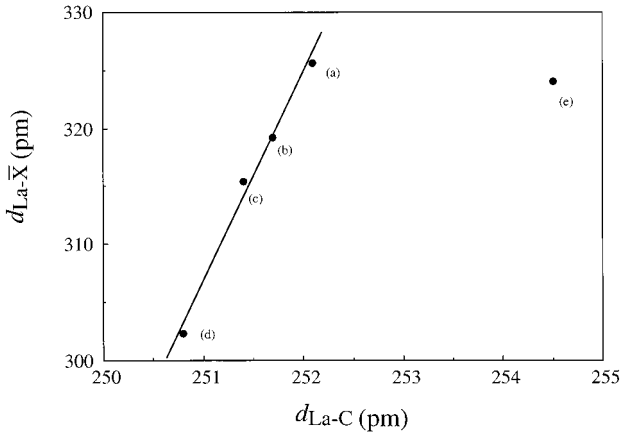

Figure 10. Mean La to halogen atom distances $d_{La-\bar{X}}$ versus the distances d_{La-C} of the axial La atom to the carbon atoms in the phases $La_2C_2(X, X')_2$. (a: 1s-$La_2C_2I_2$ (T_c = 1.60(5) K); b: 1s-$La_2C_2Br_{0.5}I_{1.5}$ (T_c = 1.65(3) K); c: 1s-$La_2C_2Cl_{0.5}I_{1.5}$ (T_c = 1.82(3) K); d: 1s-$La_2C_2Br_2$ (T_c = 7.03(5) K); e: 3s-$La_2C_2I_2$ (T_c = 1.72(5) K)).

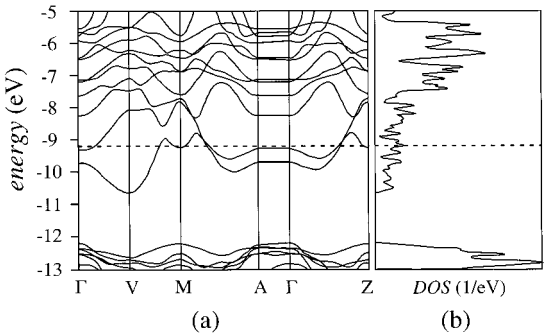

Figure 11. (a) Band dispersion for 3s-$La_2C_2I_2$ in selected directions of the Brillouin zone and (b) corresponding density of states DOS (Fermi level at −9.2 eV).

TABLE 7: Lattice Parameters and C−C Distances at 1.5 K According to Neutron Powder Diffraction of All Investigated Samples

no.	compd	type	*a* (pm)	*b* (pm)	*c* (pm)	β (deg)	d_{C-C} (pm)
2	$La_2C_2Br_2$	1s	746.09(5)	404.93(3)	1001.16(9)	94.163(5)	134.1(7)
4	$La_2C_2I_2$	1s	761.90(3)	412.52(2)	1075.13(7)	93.143(4)	132.2(5)
5	$La_2C_2I_2$	3s	761.32(2)	413.24(1)	1085.90(4)	100.835(2)	128.4(4)
6	$La_2C_2Br_{0.5}I_{1.5}$	1s	758.57(3)	409.81(2)	1067.82(5)	93.272(2)	131.5(4)
7	$La_2C_2Cl_{0.5}I_{1.5}$	1s	757.64(3)	407.58(2)	1072.66(5)	93.384(3)	129.7(5)

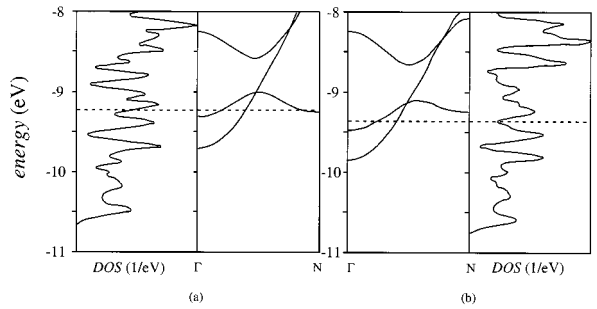

Figure 12. Density of states (DOS) and band dispersion for (a) 3s-$La_2C_2I_2$ and (b) 1s-$La_2C_2I_2$ plotted for the Γ−N (−1/2, 1/2, 0) direction in the Brillouin zone.

atomic orbital projections we assign the character of the bands as follows: (1) bands between −12.9 and −14.2 eV are mostly of I−p character and some contributions from C_2-π* levels; (2) a strong mixing of C_2-π* levels (40%) and La-d orbitals (60%) occurs between −10.8 eV and −5.3 eV; and finally (3) the broad metal d bands extend from −5.3 eV upwards (not plotted in the figure). Figure 11 shows the band dispersion curves plotted over some selected directions in the Brillouin zone. Along the direction Γ−A, the bands exhibit negligible dispersion which may be expected from the two-dimensional characteristics of the crystal structure. The local maximum in the DOS around E_F, however, rather originates from bands of low dispersion along Γ−N (= −1/2, 1/2, 0), (Figure 12). The direction Γ−N corresponds to the direction of the crystallographic *a* axis or the projection of the C−C group onto the crystallographic *a*-*b* plane. This in-plane band of low dispersion should be essential for superconductivity in these phases.[7]

From the Rietveld refinement results it is found that especially the 1s and 3s stacking variant of $La_2C_2I_2$ show a difference in the C−C bond length. C−C distances of 128.4(4) pm and 132.2-(5) pm are found for 3s- and ls-$La_2C_2I_2$, respectively (Table 7). The variation of the La−La distances of the 3s and 1s form does not exceed 0.3%. The expansion of the C_2 unit may be expected to lower the energy of the C_2-π* states and to affect the overlap of antibonding C_2-π* with La-d states. A calculation of the electronic band structure of 1s-$La_2C_2I_2$ seems to indicate that these structural changes indeed influence the position relative to E_F of the low dispersive bands along Γ−N, while we observe no significant alteration of the bands along the Γ−A direction. As a consequence of the different C and La−C interaction the DOSs near E_F calculated for identical composition (see section V) exhibit differences for 1s-$La_2C_2I_2$ and 3s-$La_2C_2I_2$. The Fermi level for 1s-$La_2C_2I_2$ comes to lie in a local minimum, while E_F for 3s-$La_2C_2I_2$ is shifted towards a local maximum. The different DOS for 3s-$La_2C_2I_2$ as compared to 1s-$La_2C_2I_2$ could be the origin of the increased superconducting transition temperature of 3s-$La_2C_2I_2$ as observed in the experiments. Volume dependent band structure calculations reveal a subtle flattening of the low dispersive band along Γ−N when the cell volume is decreased, e.g., by introducing larger halogen constituents (Figure 7).

V. Conclusions

The neutron powder diffraction investigations prove very helpful in establishing phase purity of these new superconductors. Refinement of the diffraction patterns of phase-pure samples also allows to improve the accuracy of the positional parameters of C atoms, as compared to X-ray data. The onset of superconductivity in $La_2C_2Br_2$ is found close to 7 K in a set of three samples, irrespective of details in the sample preparation.

The difference in the transition temperatures of 1s type and 3s type $La_2C_2I_2$ is unprecedented in the $Y_2C_2X_2$ phases. There, the T_cs of mixed halide samples, $Y_2C_2(X,X')_2$, pass over two changes of the stacking sequence without showing any jumps. This finding was considered as strong evidence for the assumption that the X−Y−C_2−Y−X slabs themselves are in the first place responsible for superconductivity in RE carbide halides. The difference in T_c for the 1s- and 3s-$La_2C_2I_2$ samples could point to an additional sensitivity of the electronic conditions in the I−La−C_2−La−I slabs to packing effects in the halogen atom double layer. However, the observation that pure 3s type samples of $La_2C_2I_2$ can only be prepared using a considerable excess of carbon while mixed 1s/3s type samples result when the carbon excess is reduced close to stoichiometric mixtures strongly indicates that the 1s type samples exhibit a carbon deficiency, $La_2C_{2-x}I_2$. Such a substoichiometric carbon content which is below detection level may easily be achieved by a substitution of C_2^{4-} groups by isoelectronic C^{4-} anions without noticeably altering the crystal structure. As experienced in the case of $Y_2C_2I_2$, partial replacement of C_2 by C_1 leads to a marginal decrease of the lattice parameters only, while it may induce a marked reduction of T_c.[7]

As a central result we can identify, from the band structure calculations, a band of low dispersion in the direction (Γ−N) which corresponds to the direction of the crystallographic *a* axis. We emphasize that the flat band originates from orbital interactions within the layer and not from interactions perpendicular to the layers. Hence the flat/steep band scenario in the band structure proposed to be essential for the $RE_2C_2X_2$ superconductors is not a trivial consequence of the layered character of the crystal structure of these phases.[7]

Acknowledgment. We thank E. Suard and P. Cross at the ILL for their kind assistance in the neutron experiment, E. Brücher and G. Siegle for the resistivity and susceptibility measurements, W. Röthenbach for the X-ray powder diffraction measurements.

References and Notes

(1) Simon, A.; Mattausch, Hj.; Eger R.; Kremer, R. K. *Angew. Chem., Int. Ed. Engl.* **1991**, *30*, 1188.

(2) Schwanitz-Schüller, U.; Simon, A. *Z. Naturforsch. B* **1985**, *40*, 710.

(3) Mattausch, Hj.; Kremer, R. K.; Eger, R.; Simon, A. *Z. Anorg. Allg. Chem.* **1992**, *609*, 7.

(4) Yamanaka, S.; Hotehama, K.; Kawaji, H. *Nature* **1998**, *392*, 580.

(5) Kawaji, H.; Hotehama, K.; Yamanaka, S. *Chem. Mater.* **1997**, *9*, 2127.

(6) Yamanaka, S.; Kawaji, H.; Hotehama, K.; Ohashi, M. *Adv. Mater.* **1996**, *8*, 771.

(7) Simon, A.; Yoshiasa, A.; Bäcker, M.; Henn, R. W.; Felser, C.; Kremer, R. K.; Mattausch, Hj. *Z. Anorg. Allg. Chem.* **1996**, *622*, 123.

(8) Simon, A. *Angew. Chem.* **1997**, *109*, 1879; *Angew. Chem., Int. Ed. Engl.* **1997**, *36*, 1788.

(9) Henn, R. W. Dissertation Thesis, University Karlsruhe (TH), 1996.

(10) Henn, R. W.; Schnelle, W.; Kremer, R. K.; Simon, A. *Phys. Rev. Lett.* **1996**, *77*, 374.

(11) Bäcker, M.; Simon, A.; Kremer, R. K.; Mattausch, Hj.; Dronskowski, R.; Rouxel, J. *Angew. Chem., Int. Ed. Engl.* **1996**, *35*, 752.

(12) Bäcker, M. Dissertation Thesis, University Stuttgart, 1997.

(13) Herrling, E.; Dormann, E.; Henn, R. W.; Kremer, R. K.; Simon, A. *Synth. Met.* **1998**, *92*, 13.

(14) Gulden, Th. Dissertation Thesis, University Stuttgart, 1997.

(15) Gulden, Th.; Henn, R. W.; Jepsen, O.; Kremer, R. K.; Schnelle, W.; Simon, A.; Felser, C. *Phys. Rev.* **1997**, *B56*, 9021.

(16) Miller, G. J.; Burdett, J. K.; Schwarz, C.; Simon, A. *Inorg. Chem.* **1986**, *25*, 4437.

(17) Henn, R. W.; Strach, T.; Kremer, R. K.; Simon, A. *Phys. Rev.* **1998**, *B58*, 14346.

(18) Ahn, K.; Mattausch, Hj.; Simon, A. *Z. Anorg. Allg. Chem.* **1997**, *623*, 619.
(19) Taylor, M. D.; Carter, C. P. *J. Inorg. Nucl. Chem.* **1962**, *24*, 387.
(20) Meyer, G.; Ax, P. *Mat. Res. Bull.* **1982**, *17*, 1447.
(21) Krause, B. H.; Hook, A. B.; Warner, F. *Acta Cryst.* **1963**, *16*, 848.
(22) Simon, A. *J. Appl. Crystallogr.* **1970**, *3*, 11.
(23) Izumi, F. *The Rietveld Method*; Young, R. A., Ed.; University Press: Oxford, 1993; Chapter 13.
(24) Hoffmann, R. *J. Chem. Phys.* **1963**, *39*, 1397.
(25) Whangbo, M.; Hoffmann, R. *J. Am. Chem. Soc.* **1978**, *100*, 6093.
(26) Kremer, R. K.; Ahn, K.; Henn, R.; Mattausch, Hj.; Schnelle, W.; Stolovits, A.; Simon, A. Conference Proceedings of the 1st Conference on Anomalous and Complex Superconductors, to appear in *Physica C*.
(27) Gratz, E.; Zuckerman, M. J. *Handbook of the Physics and Chemistry of Rare Earth*; Gschneider, K. A., Jr., Eyring, L., Eds.; North Holland, 1982; Chapter 42.
(28) Coleman, R. V.; Eiserman, G. K.; Hillenius, S. J.; Mitchell, A. T.; Vincent, J. L. *Phys. Rev.* **1983**, *B27*, 125.
(29) Oshima, K.; Urayama, H.; Yamochi, H.; Saito, G. *Physica* **1988**, *153−155C*, 1148.
(30) Bauhofer, W.; Biberacher, B.; Gegenheimer, B.; Joss, W.; Kremer, R. K.; Mattausch, Hj.; Müller, A.; Simon, A. *Phys. Rev. Lett.* **1989**, *63*, 2520.
(31) Pauling, L. *The Nature of the Chemical Bonding*; Cornell University Press: Ithaca, New York, 1960.